Liquid Crystals
Publication details, including instructions for authors and subscription information:
http://www.informaworld.com/smpp/title~content=t713926090

The stability diagram of a nematic liquid crystal confined to a cylindrical cavity

S. Kralj[a]; S. Žumer[b]
[a] Faculty of Education, University of Maribor, Koroška, Slovenia [b] Department of Physics, University of Ljubljana, Jadranska, Slovenia

To cite this Article Kralj, S. and Žumer, S.(1993) 'The stability diagram of a nematic liquid crystal confined to a cylindrical cavity', Liquid Crystals, 15: 4, 521 — 527
To link to this Article: DOI: 10.1080/02678299308036471
URL: http://dx.doi.org/10.1080/02678299308036471

LIQUID CRYSTALS, 1993, VOL. 15, NO. 4, 521–527

The stability diagram of a nematic liquid crystal confined to a cylindrical cavity†

by S. KRALJ*‡ and S. ŽUMER§

‡ Faculty of Education, University of Maribor, Koroška 160, Slovenia
§ Department of Physics, University of Ljubljana, Jadranska 19, Slovenia

(*Received 16 September 1992; accepted 20 May 1993*)

Different nematic structures confined to a long cylindrical cavity with homeotropic surface anchoring are studied using a numerical minimization of the free energy of the uniaxial nematic liquid crystal. The stability of escaped radial structures and planar polar structures (with and without line defects) is analysed in terms of the ratio of elastic constants K_{24}/K_{11}, K_{33}/K_{11}, anchoring strength and external magnetic field applied perpendicular to the symmetry axis of the cylinder. We draw the analogy between the stability diagram of the cylindrical structures and structures in a spherical droplet. In particular, a simple way extracting the value of the saddle-splay elastic constant K_{24} from the stability studies is discussed.

1. Introduction

Recently there have been a number of experimental and theoretical studies devoted to nematic liquid crystals (NLC) confined to cylindrical environments [1–6]. This interest arises from the relevance of micro-confined systems to electro-optical applications and because these systems are very suitable for studies of elastic anchoring properties of liquid crystals. In particular, in such systems, the saddle-splay elastic constant K_{24} has been experimentally determined for the first time [3].

Different nematic structures within a cylindrical cavity can be in most cases well presented by a director field $\hat{\mathbf{n}}(\hat{\mathbf{r}})$ pointing along an average local orientation of nematic molecules. The director field inside a cavity is a result of the competition between the surface anchoring potential, elastic forces and external electric or magnetic field. In a system with homeotropic anchoring, where the surface interactions tend to align the nematic molecules along the normal to the surface, the escaped radial (ER) [1] and planar polar (PP) [4] structures have been observed. Using the approximation of equal Frank elastic constants, the stability diagram of these structures in a zero enternal field was studied first by Allender *et al*, [3, 4].

The aim of this paper is to describe briefly a more general stability diagram for nematic structures in a long cylindrical cavity where variations of the anchoring strength, external magnetic field, and ratios of the elastic constants K_{24}/K_{11}, and K_{33}/K_{11} are taken into account. Particular attention is paid to the comparison of the resulting stability diagram to the one corresponding to spherical droplets with homeotropic boundary conditions. A more detailed study of nematic structures in cylindrical cavities will be given elsewhere [7].

* Author for correspondence.

† Presented at the Fourteenth International Liquid Crystal Conference, 21–26 June 1992, University of Pisa, Italy.

0267-8292/93 $10·00

2. Free energy

The stable nematic structures in micron or supra-micron size cavities are determined by a minimization of the free energy contributions [8, 9]

$$f(\mathbf{r})=\frac{K_{11}}{2}(\operatorname{div}\mathbf{n})^2+\frac{K_{22}}{2}(\hat{\mathbf{n}}.\operatorname{rot}\hat{\mathbf{n}})^2+\frac{K_{33}}{2}(\hat{n}\times\operatorname{rot}\hat{\mathbf{n}})^2$$

$$-\frac{K_{24}}{2}(\hat{\mathbf{n}}\times\operatorname{rot}\hat{\mathbf{n}}+\hat{\mathbf{n}}\operatorname{div}\hat{\mathbf{n}}).\hat{\mathbf{e}}_{\text{surf}}\delta(\hat{\mathbf{r}}-\hat{\mathbf{R}})+\frac{K_{11}}{2d}(\hat{\mathbf{n}}.\hat{\mathbf{e}}_{\text{easy}})^2)\delta(\hat{\mathbf{r}}-\hat{\mathbf{R}})-\frac{K_{11}}{2\xi^2}(\hat{\mathbf{n}}.\hat{\mathbf{e}}_{\text{field}})^2 \qquad (1)$$

containing the elastic part characterized by the elastic constants K_{11}, K_{22}, K_{33}, K_{24}, the magnetic field (**B**) part characterized by the correlation length $\xi=\sqrt{[K_{11}\mu_0(\mathbf{B}^2\chi)]}$ [8] ($\Delta\chi$ is the anisotropy of the magnetic susceptibility along $\hat{\mathbf{n}}$ and perpendicular to it), and the surface interaction part characterized by the coherence length $d=K_{11}/W_0$ [8] (W_0 is the anchoring strength). The term $\hat{\mathbf{e}}_{\text{easy}}$ stands for the preferred anchoring direction (*'easy'* direction), $\hat{\mathbf{R}}$ for the radius vector describing the confining surface, and $\hat{\mathbf{e}}_{\text{surf}}$ for the normal to that surface. In the case of homeotropic anchoring, we have: $\hat{\mathbf{e}}_{\text{easy}}\|\hat{\mathbf{e}}_{\text{surf}}$. We limit our study to the case $\Delta\chi>0$ and to structures without twist deformations. Further, only cases with magnetic field perpendicular to the symmetry axes of the cylinders are discussed. Minimization of the free energy in the same way as for droplets [10] leads to bulk and surface differential equations. Differential equations are solved numerically using the over-relaxation method. In the next section we present our main results but leave the details to be presented elsewhere [7].

3. Results and discussion

The PP and ER nematic structures, which are most often stable in cylindrical cavities where the wall enforces homeotropic anchoring, are schematically presented in figures 1 (*a*) and (*b*). The resulting director patterns in the plane perpendicular to the symmetry axis of the cylinder are similar to the axial (AX) and radial (RA) director fields of a spherical nematic droplet [10]. To explore these similarities, the stability diagrams of predicted nematic structures in cylindrical and spherical cavities are shown together in figure 2. They also show a qualitative similarity for comparable values of the elastic constants ($K_{11}\sim K_{33}\sim K_{24}$). The RA and ER structures are stable in the regime of strong anchoring and weak external field because they have smaller surface free energy than AX and PP structures. The latter are stable in the weak anchoring regime and for any anchoring strength in a strong external field, because of lower bulk contributions to the elastic and field parts of the free energy. Further, our calculations show that, as for nematic droplets, where axial structures with a circular line defect (AXDL) can be stable [10], in a cylindrical cavity too a planar polar structure with two line defects of strength 1/2 running along the symmetry axes of the cylinders (PPDL- see figure 1 (*c*)) can be stable. To our knowledge, this structure has not yet been experimentally observed. It should be stressed that, because of the presence of the defects, the coexistence curves (see figure 2) separating stability regions of structures with line defects and without them depend also on the cavity radius R itself [7, 10], and not only on the ratios R/d, R/ξ which enter the Euler–Lagrange equations [7]. Besides this, it should be mentioned that calculations show that the external field negligibly affects the director field of ER structures as long as $R/\xi<3$. Therefore, our coexistence curves, which are all well below this value, have been calculated in the approximation of the undeformed director field.

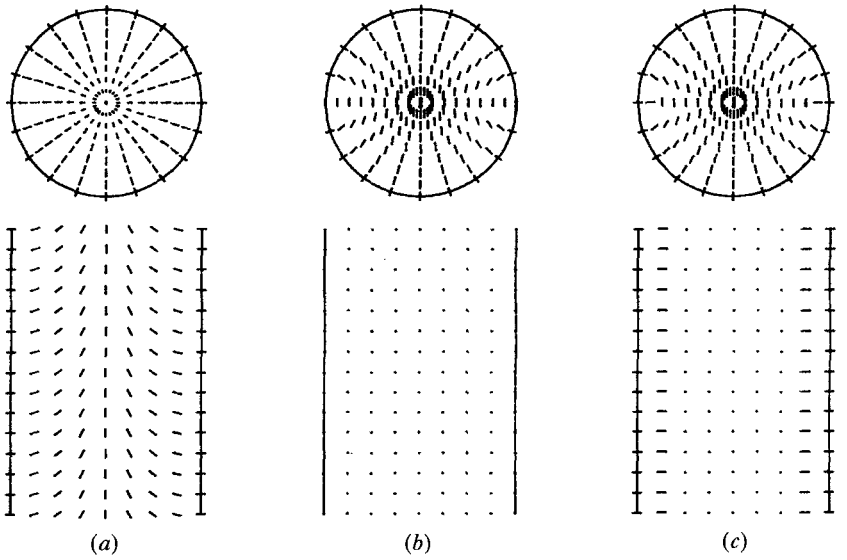

Figure 1. The nematic director field of (*a*) an escaped radial, (*b*) a planar polar and (*c*) a planar polar structure with two line defects realized in a cylindrical cavity. The length of lines representing the director field is proportional to the component of the director field component in the cross-sectional plane.

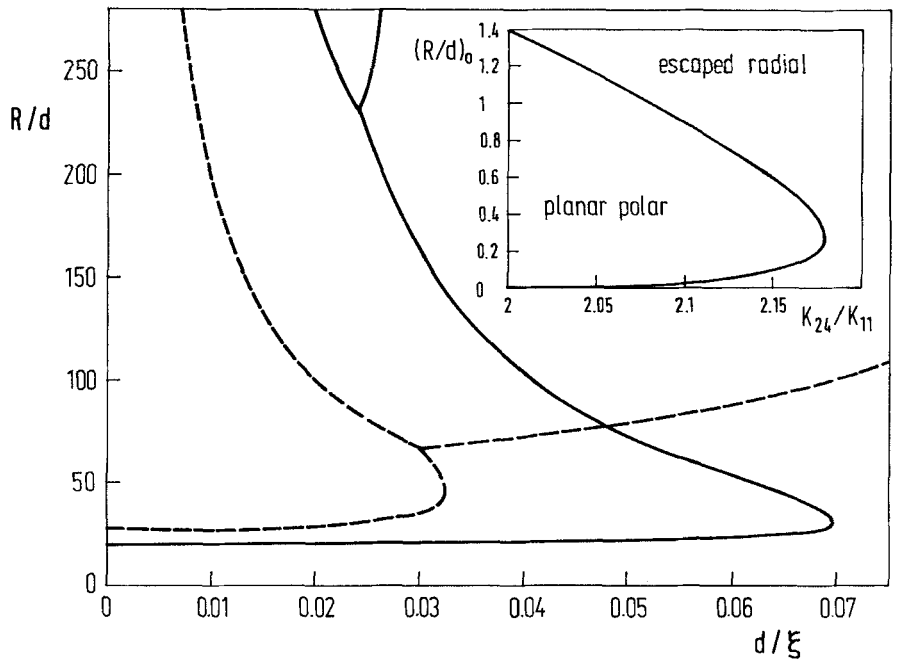

Figure 2. The stability diagrams for the planar polar (PP) structure, the planar polar structure with two line defects (PPLD), and the escaped radial structure (ER) in a cylindrical cavity (dashed line), and for the axial (AX), axial with line defect (AXLD) and radial (RA) structure in a spherical droplet (full line). The variables $R/\mathbf{d}$ and d/ξ measure anchoring and the external field strength, respectively. In calculations, we set $K_{24}=0$, $K_{33}=K_{11}$. The PP and AX structures are stable in the weak anchoring regime, the ER and RA structures in the strong anchoring regime, and in a finite interval of external field strengths, the PPLD and AXLD structure can be stable. In the inset, the stability diagram of the PP and ER structure for different anchoring strengths and ratios $K_{24}/K_{11}>2$ is shown for $K_{33}=K_{11}$ and zero external field.

The main differences between stability diagrams for spherical and cylindrical cavities are:

(i) The zero field coexistence point $(R/d)_0$ separating stability regions of the PP and ER structures lies significantly higher than $(R/d)_0$ for a AX to RA transition. This is caused by the relatively larger surface to volume ratio in droplets.

(ii) In cylindrical cavities, the inversion point, (i), where the coexistence line reaches its maximum value $(d/\xi)_i$, occurs at smaller values of the ratio (d/ξ) than in droplets. This indicates that the external field stabilizes PP structures more than AX structures.

(iii) The PP structure with line defects can be stable at lower values of the ratio R/d than for the AXDL structure, because of the relatively smaller volume occupied by defect lines in cylindrical cavities.

The dependence of the stability diagram on the elastic properties of liquid crystals is shown in figure 3. We begin by considering the the influence of the K_{33}/K_{11} ratio. The PP structures have more bend deformation than ER structures. In spherical droplets, the splay deformation is dominant in the axial structure, particularly in low magnetic fields. The effect of the saddle splay constant K_{24} is present in the free energy of ER, AX and RA structures, but absent in the PP structure where $\mathrm{div}(\hat{\mathbf{n}} \times \mathrm{rot}\,\hat{\mathbf{n}} + \hat{\mathbf{n}}\,\mathrm{div}\,\hat{\mathbf{n}})$ equals zero. If $K_{24} > 0$ then the K_{24} term prefers radial-like structures and its influence on the stability diagram is larger in droplets because of the larger surface to volume ratio.

Bigger differences between stability diagrams for nematic structures confined to spherical and cylindrical cavities appear at large K_{24} values (see the insert to figure 2

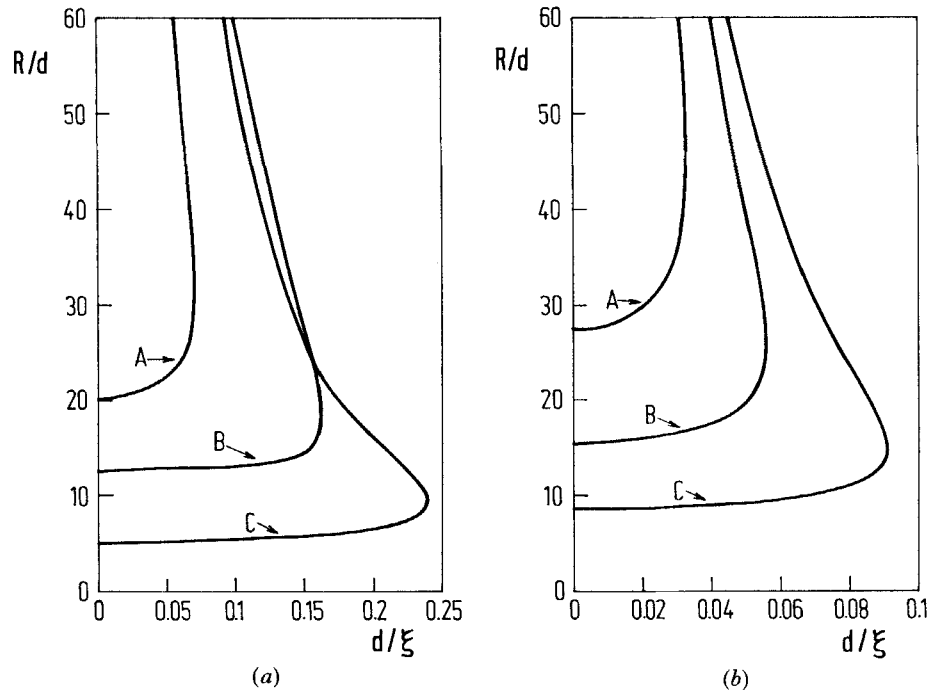

Figure 3. Effect of elastic constants K_{11}, K_{33} and K_{24} on the stability diagram for (*a*) a spherical and (*b*) a cylindrical cavity of NLC. A, $K_{33}/K_{11} = 1$ and $K_{24}/K_{11} = 0$; B, $K_{33}/K_{11} = 2$ and $K_{24}/K_{11} = 0$; C, $K_{33}/K_{11} = 1$ and $K_{24}/K_{11} = 1$.

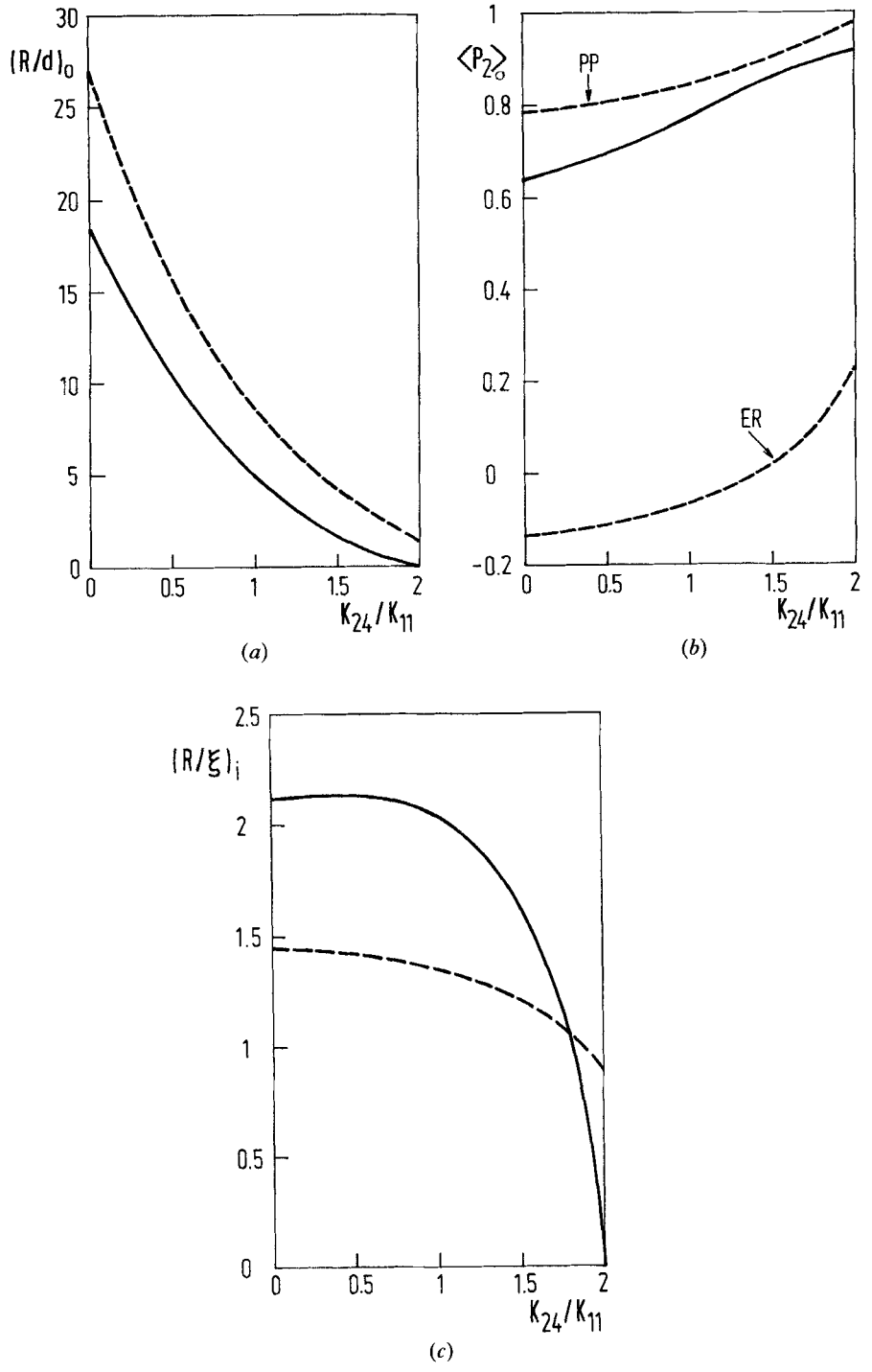

Figure 4. The K_{24} dependence of (*a*) the zero field coexistence point $(R/d)_0$, (*b*) the corresponding $\langle P_2 \rangle$ value of the PP, ER and AX structures and (*c*) the inversion point value $(R/\xi)_i$. The dashed line denotes the cylindrical and the full line the spherical cavity. $K_{33}/K_{11}=1$.

where the zero external field diagram is shown for $K_{33}/K_{11}=1$!). In the cylinder, an additional region where ER structures are stable appears for $K_{24}/K_{11}>2$. In the weak anchoring regime and above $K_{24}/K_{11}\sim 2{\cdot}18$, this nematic director configuration is stable for all anchoring strengths. For the same K_{33}/K_{11} ratio, the zero field coexistence point in a spherical droplet reaches the value $(R/\mathrm{d})_0=0$ at $K_{24}/K_{11}=2$.

Recently, a lot of effort have been given to finding an appropriate experimental method enabling the determination of the K_{24} elastic constant [3, 4, 10, 11] and the anchoring strength W_0. The strong dependencies of confined structures and their stability diagrams on the elastic and anchoring properties of nematic liquid crystals can be used for the determination of these properties. An NMR line study of the ER structures has enabled the first determination of the elastic constant K_{24} [3]. In a new paper [11], we discuss, in detail, two possible ways of extracting the K_{24} and W_0 values from a stability diagram for a spherical droplet: (i) from the position of the zero field coexistence point $(R/d)_0$ and (ii) from the value $(R/\xi)_i$ at the inversion point. Here we extend this approach to cylinders and compare the predicted dependencies of $(R/d)_0$, $\langle P_2\rangle_0$ ($\langle P_2\rangle$ at $(R/d)_0$), and $(R/\xi)_i$ on K_{24} for both geometries. The order parameter of a structure $\langle P_2\rangle=\langle(3(\hat{\mathbf{n}}(\hat{\mathbf{r}}).\hat{\mathbf{e}})^2-1)/2\rangle$, where $\langle\ldots\rangle$ stands for the average over a cavity volume and $\hat{\mathbf{e}}$ points along the symmetry axis of the structure, reflects general features of the nematic director field within a cavity. The radius of cylinders or droplets corresponding to the zero field coexistence point and inversion point are usually in the submicron range, therefore NMR is the best method to determine $\langle P_2\rangle$. This is not the case for the observation of the inversion point, where one needs an additional variable external field which cannot be easily realized in the NMR apparatus. Once $\langle P_2\rangle_0$ is experimentally determined, then using the corresponding theoretically predicted behaviour of $\langle P_2\rangle_0$ (see figure 4(*b*) for ER or PP structures in cylinders and AX structures in droplets, the ratio K_{24}/K_{11} can be estimated. In the next step, using K_{24}/K_{11} and the theoretically predicted behaviour of the zero-field coexistence curve (see figure 4(*a*)), the value of the anchoring strength W_0 can be extracted. The determination of K_{24} and W_0 from $\langle P_2\rangle$ which is directly proportional to the NMR line splitting is simpler than a determination from a precise fit of the NMR line shapes. The disadvantage of the proposed method is the possible occurrence of metastable structures.

4. Conclusion

We have determined the stablity regions of the escaped radial and planar polar nematic structures confined to a cylindrical cavity for different external magnetic field strengths, anchoring strengths and ratios of the elastic constants K_{24}/K_{11}, K_{33}/K_{11}. We have shown that the stability diagram is qualitatively similar to the one obtained for a spherical droplet, where radial and axial structures compete. Qualitative differences between stability diagrams for spherical cylindrical environments appear for large K_{24} elastic constants. We have shown that the stability diagram can be used for an indirect study of the elastic and anchoring properties of nematic liquid crystals. A more detailed analysis of these phenomena for cylindrical cavities is in progress and will be published elsewhere.

References

[1] Cladis, P. E., and Kleman, M., 1972, *J. Phys. Paris*, **33**, 591.
[2] Vilfan, I., Vilfan, M., and Žumer, S., 1991, *Phys. Rev.* A, **43**, 6875.
[3] Allender, D. W., Crawford, G. P., and Doane, J. W., 1991, *Phys. Rev. Lett.*, **67**, 1442.

[4] ALLENDER, D. W., CRAWFORD, G. P., and DOANE, J. W., 1992, *14th International Liquid Crystal Conference, Pisa*, Abstracts p. 373.
[5] CRAWFORD, G. P., STANNARIUS, R., and DOANE, J. W., 1991, *Phys. Rev.* A, **44**, 2558.
[6] CRAWFORD, G. P., CRAWFORD, R. O., ŽUMER, S., and DOANE, J. W., 1992, *14th International Liquid Crystal Conference, Pisa*, Abstracts, p. 375.
[7] ŽUMER, S., and KRALJ, S. (in preparation).
[8] DE GENNES, P. G., 1974, *The Physics of Liquid Crystals* (Oxford University Press).
[9] SAUPE, A., 1981, *J. chem. Phys*, **75**, 5118.
[10] KRALJ, S., and ŽUMER, S., 1992, *Phys. Rev.* A, **45**, 2461.
[11] ŽUMER, S., and KRALJ, S., 1992, *Liq. Crystals*, **12**, 613.